Automatika

Journal for Control, Measurement, Electronics, Computing and Communications

ISSN: (Print) (Online) Journal homepage: www.tandfonline.com/journals/taut20

A novel solar photo voltaic powered drive for the SRM for irrigation purposes using a partial resonant AC link DC to a DC boost converter

R. Kalai Selvi & R. Suja Mani Malar

To cite this article: R. Kalai Selvi & R. Suja Mani Malar (2023) A novel solar photo voltaic powered drive for the SRM for irrigation purposes using a partial resonant AC link DC to a DC boost converter, Automatika, 64:4, 903-918, DOI: 10.1080/00051144.2023.2225343

To link to this article: https://doi.org/10.1080/00051144.2023.2225343

Published online: 06 Jul 2023.

AUTOMATIKA
2023, VOL. 64, NO. 4, 903–918
https://doi.org/10.1080/00051144.2023.2225343

A novel solar photo voltaic powered drive for the SRM for irrigation purposes using a partial resonant AC link DC to a DC boost converter

R. Kalai Selvi[a] and R. Suja Mani Malar[b]

[a]Department of Electrical and Electronics Engineering, PET Engineering College, Vallioor, India; [b]Department of Electrical Electronics and Communication Engineering, National Institute of Technical Teachers' Training and Research, Taramani, India

ABSTRACT

In this study a novel drive for the Switched Reluctance Motor (SRM), powered by the solar photo voltaic (SPV) source, using a Partial Resonant Inverter (PRI) followed by a Doubler Rectifier (DR) for water pumping applications, has been proposed and validated. The PRI DR combination offers a large voltage gain that is required while using low-voltage SPV sources. The PRI increases the voltage level by resonance and also it exhibits zero voltage switching so that the switching losses are reduced. The proposed system also offers a sliding mode controller based on Maximum PowerPoint Tracking implemented in the PRI. The proposed system is a fixed torque variable speed application where the speed follows the solar irradiance. The proposed idea has been validated using simulations and experimental prototypes.

ARTICLE HISTORY
Received 23 April 2023
Accepted 9 June 2023

KEYWORDS
Partial resonance inverter; double rectifier; solar photo voltaic energy; sliding mode controller; maximum power point tracking; switched reluctance motor

1. Introduction

Despite the intermittent nature of solar energy, PV panels are a viable alternative energy source in many domestic, commercial or industrial applications (basically for self-consumption), from decentralized power generation to supply isolated loads to even connected to the local distribution network. Water pumping systems for people, animals or flora, as well as irrigation canals in agriculture, are key applications where solar energy can be utilized. It makes sense that there are so many water pumping facilities in the world given that water is one of the most necessary resources for human survival, national sustainability and global sustainability. Photovoltaic solar systems are useful for this in a variety of ways, particularly when used in rural locations where there is no electrical supply or where building such infrastructure would be expensive [1–4]. The SRM is a single-excited electromechanical system which can be used for high-speed industrial rotary applications. Like the Permanent Magnet Brushless DC motor the SRM motor has no brushes because it has neither a winding nor a set of permanent magnets in the rotor. The SRM does not use permanent magnets and it should be cheaper compared to the brushless DC motor. Even though the SRM is of a simple structure it had not become popular in the industrial environment because the SRM requires a special mechanical rotational position sensor of the shaft and a sequential switching circuit that energizes the timely selected winding from the available phase windings of the SRM. The SRM requires a DC voltage source and a power electronic switching circuit. The torque produced by the SRM is a function of the current flows through the active winding phase and the position of the approaching metal pole that is mounted in the rotating shaft of the motor.

The contribution of this paper is as follows.

- To design a novel drive for the Switched Reluctance Motor (SRM) powered by the solar photo voltaic (SPV) source using a Partial Resonant Inverter (PRI) followed by a Doubler Rectifier (DR) for water pumping applications
- To implement sliding mode controller-based Maximum Power Point Tracking in a Partial Resonant Inverter
- The proposed system has been validated using simulations and experimental prototypes.

The article has been organized as follows. The related work is given in section 2. The outline of the proposed work and its circuit details are presented in section 3. The MATLAB SIMULINK based on circuit modelling and the results of simulations are presented in section 4. An experimental prototype was developed and the details are presented in section 5. In section 6, the conclusion and the references sections are included.

2. Related work

A proliferation of research articles has come up in the recent past and consideration of these articles reveals the research gap. Some of the important contributions

CONTACT R. Kalai Selvi kalaiselvir.eee@gmail.com, kalaiselvi946@gmail.com Department of Electrical and Electronics Engineering, PET Engineering College, Vallioor, Tamilnadu 627117, India

are outlined here. In the research article presented as [5] the authors have presented a detailed mathematical modelling of the SRM. This work can be considered as a starting point for carrying out further research in SRM. The textbook on electrical machines by the authors in [6,7] also provides the reader with a clear insight into the principles of electrical machines. Such as in [8] many authors have made valuable contributions to the design, comparison of various designs and the control of the SRM. A novel SRM with toroidal windings and a 6-switched drive for the SRM was proposed, designed, developed and demonstrated by the authors in [9]. A high-speed SRM for applications in electric vehicles was proposed and validated by the authors in [10]. The authors in reference [11] have claimed the successful development of an optimally designed SRM that is fed by an asymmetric bridge-type power electronic converter. The authors in [12] have developed a novel SRM design procedure that took into consideration the analysis of harmonics and back emf and the design was focused on developing a traction scheme for the electrical vehicle. An analysis of the state-of-the-art developments that have happened about the SRM-based power trains and their drive for applications in electric vehicles [13]. A review of the research trends and an overview pertaining to the SRM were developed by the authors in [14]. Furthermore, a four-quadrant drive for the SRM has been proposed and validated by the authors in [15].

Contemporarily there had been many developments in the field of SPV energy harvesting systems and these systems have also contributed to the development of electric drives in areas unconnected to the national grid and are thus contributing to the development of irrigation pumps. In a typical development the authors in [16] have developed a novel battery charging unit that has used an intelligent Maximum Power Point Tracking of the SPV energy harvesting system. In article [17] the future potential of solar-powered pumps has been studied based on the review of past articles on renewable energy harvesting systems. The development of mathematical modelling of the SPV cell had also been an attraction for many scientists and a similar development with single and double diode models of the SPV cell was presented by the authors in [18]. To enhance the efficiency of an SPV panel a nanocomposite thermal regulator was proposed and validated by the authors in [19]. This work is an example of the various developments happening in the material science of the solar photo voltaic panel.

[20] is a detailed study of the optimal sizing of the solar and wind energy units for a hybrid renewable energy scheme that focuses on the economic and social perspectives of the state of the renewable energy systems.

Maximum power point tracking is also considered an important research area and many scholars have contributed to a proliferation of articles in a similar development the authors in [21] have presented the design and implementation procedure of the Perturb and Observe MPPT algorithm for the solar photo voltaic source. Grid integration of renewable energy systems including SPV energy had also been a deeply researched area and the authors in [22] have developed a novel control algorithm for the grid integration of the SPV source to the national grid. An adaptive DC link voltage-dependent grid integration of the SPV source had been proposed designed and validated by the authors in [23].

Resonant inverters and partial resonant inverters have also entered into the power conversion arena and the partial resonant power converters are reported by some authors claiming certain specific advantages. In a typical development the authors in [24] have presented a grid-integrated distributed generation system with the help of a Soft Switched Partial Resonance Inverter.

The authors in [25] have presented a voltage equalizer system based on a two-switch configuration with an LLC resonant inverter followed by a voltage multiplier. The authors have developed the proposed system to manage partially shaded conditions applicable to a string of photovoltaic modules. A sliding mode controller-based MPPT for the harvest of SPV source used with a PRI followed by a doubler rectifier has been presented in [26]. In another development [27] a bidirectional partial resonant AC link converter has been proposed and validated. A similar application of the PRI for harvesting renewable energy has been proposed and validated by the authors in [28]. The authors in [29] have presented an elaborate analysis of the modern series and parallel resonant inverters and converters for applications in solar power harvesting. The authors in [30] have developed a voltage equalizer system using an inverter developed with a set of two switches and a partially resonant series inverter along with a voltage multiplier specifically for use in SPV systems subjected to partially shaded solar irradiance. A novel series resonant inverter with a current regulation scheme for the pulse width modulation had been proposed and validated by the authors in [31–32].

A careful consideration of the available literature reveals that an unmanned agricultural farm water pumping system based on the SRM powered by a low-voltage SPV source may be developed using a PRI as an interfacing converter for lifting the voltage level of the source to suit the operating voltage level of the SRM. In this article a novel SPV-powered water pumping system with an SRM through a PRI and voltage doubler chain has been presented.

The article has been organized as follows. This introduction is given in section 1. The outline of the proposed work and its circuit details are presented in section 2. The MATLAB SIMULINK based on circuit modelling and the results of simulations are presented

in section 3. An experimental prototype was developed and the details are presented in Sections 4 and 5. In Section 6, the conclusion and the references sections are included.

3. Outline of the proposed system

The proposed work uses an SPV source, a PRI, a doubler rectifier and the drive for the SRM. The block diagram of the proposed system is shown in Figure 1. The SRM requires an operating voltage of 200 V and the solar PV source has a terminal voltage of the order of 40 V. A voltage boost converter is required and the PRI acts as a boost converter and it provides a large voltage gain but the output of the PRI is a partially resonant high-frequency AC. A doubler rectifier is used after the PRI to rectify the high-frequency AC and deliver a voltage-doubled DC output. The output of the doubler rectifier is supplied to the SRM drive.

The block schematic of the proposed system is shown in Figure 1.

3.1. A review of the switched reluctance motor

A Switched Reluctance Motor has a stator and a rotor and the typical structure is shown in Figure 2. There are different models of SRM based on the number of stators and the rotor poles the two popular types of the SRM are of type 6/4 or 8/6 etc. where there are 8 stator poles and 6 rotor poles in the case of the 8/6 machine.

The stator and the rotor of the SRM have salient poles and hence the SRM is categorized as a double salient machine. The stator and the rotor poles

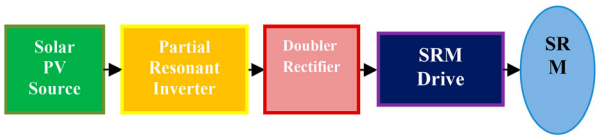

Figure 1. Block diagram of the proposed system.

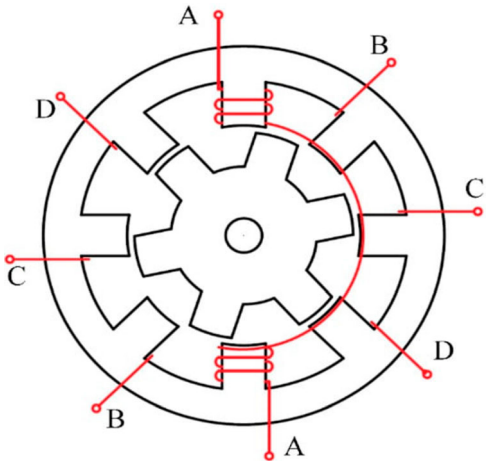

Figure 2. Structure of a switched reluctance motor.

of the SRM are made up of laminated stampings of the required shape. The salient poles of the rotor do not carry any winding while the poles of the stator have windings. The rotor poles are mounted angularly equidistant on the rotor shaft and the structure is held by bearings. The rotor shaft is free to move. The information regarding the angular position of the shaft is sensed by a position sensor the position sensor may be of the Hall Effect type or the opto coupler type. The windings on the poles of the stator are energized sequentially based on the information obtained from the position sensor. A power electronic converter governed by a micro-controller following the information from the position sensor is used to energize the stator pole windings of the SRM.

The SRM is a single excited system and the magnitude of the torque produced is a function of the path of the magnetic flux. The stator poles are stationary. As the rotor poles move along the reluctance of the magnetic path for the stator flux varies following the position of the moving rotor pole.

The basic theory of energy transfer between systems may be considered. If a finite quantity of energy is supplied to the stator phase winding a portion of the energy supplied is stored in the stator poles. The remaining portion of the supplied energy is consumed for the mechanical displacement caused. These two portions of energy are known as the "Energy" and "Co-Energy". The mechanical displacement of the rotor pole is caused by the co-energy.

The torque produced is a function of the ratio of the change in "Co-Energy" denoted as δE' to the change in rotor position $\delta\theta$. In the characteristics relating to the flux linkage and the current through the winding, the area under the magnetization curve is the co energy. The expression of torque can be given as Equation (1)

$$\text{Torque} = \frac{\delta E'}{\delta\theta} \tag{1}$$

Thus in the SRM which is a single excited system, there is only one exciting coil and the change of flux linkage is a function of θ and the current is a constant. That is $\lambda\ (\theta) = L(\theta) * I$; I is the stator current and L is the inductance of the coil. Θ is the angle between the axis of the stator pole and the axis of the rotor pole. The torque is given in (2)

$$T = \frac{\partial E'}{\partial\theta} \tag{2}$$

The mechanical work done $= \delta E_m = \delta E^2$.

E_m and E are the mechanical work done and the stored energy, respectively.

As θ changes, the stored magnetic energy and the Co energy or work done are equal. The sharing is given in Equation (3)

$$Wf = W' = 1/2L\theta * I2 \tag{3}$$

The electromagnetic torque is given in Equation (4)

$$Te = {}^{1}/_{2}(I2\delta L/\delta\theta) \tag{4}$$

3.2. Solar photovoltaic source

The proposed system uses a solar photovoltaic source for driving the SRM. The solar PV sub-system comprises six panels arranged in a set of three parallel strings with two panels in each string. The specifications of the SPV source are given in Table 1.

The SPV source can supply a maximum power of 750 W. The characteristics of the SPV sub-system is shown in Figure 3. With regard to Figure 3 the maximum power is obtained for the given solar irradiance of 1000 W/m^2 if and only if the terminal voltage of the SPV sub-system is maintained at the optimal voltage of 34.38 V. If the load is adjusted in such a manner that the terminal voltage is 34.38 then the SPV subsystem delivers maximum power to the load. For other irradiances the load should be automatically adjusted such that the terminal voltage is maintained optimal for that solar irradiance. The methodology to harvest maximum power from the SPV sub-system for all solar irradiances in an automated manner is known as maximum power point tracking. While many MPPT techniques are available such as the perturb and observe algorithm and the incremental conductance algorithm the sliding mode control method of MPPT is advantageous and it is implemented in this work. The flow chart of the SMC-based MPPT is shown in Figure 4.

Table 1. Specifications of the SPV module.

Parameter	Specification
SPV module	2 in series; 3 parallel
Nominal power rating	125.1 W
Open circuit voltage	21.58 V
Short circuit current	7.89 A
Voltage at P_{max}	17.19 V
Current at P_{max}	7.28 A

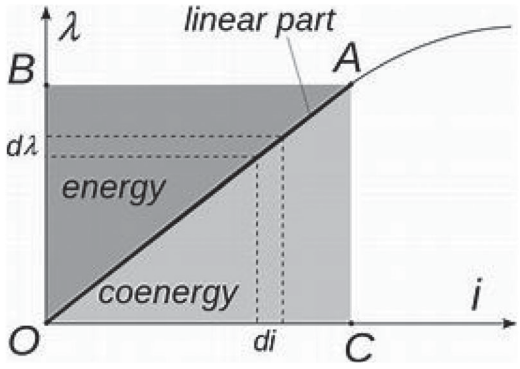

Figure 3. The characteristics of the solar PV system.

3.3. Partial resonant inverter

A PRI produces an AC voltage output that resonates at a frequency decided by the values of the L and C of the parallel resonant network placed across the output of the inverter circuit. The topology of the PRI is a part of the complete circuit diagram shown in Figure 5.

The PRI is formed using a set of four power electronic switches and four diodes. The DC input to the inverter is connected to the nodes of the PRI Bridge and the AC output is available across the rails of the PRI Bridge.

The switches S1, S2, S3 and S4 are grouped into two. The group consisting of switches S1 and S2 and the other group consisting of S3 and S4 have switched alternately at the switching frequency of 8460 Hz. The frequency of the carrier is decided by the values of the L and C used in the AC link, as shown in Equation 5.

$$F = 1/(2\pi\sqrt{LC}) \tag{5}$$

With a value of $L = 50$ micro-Henry and a capacitor of 0.2 μF the frequency of the carrier was decided at 8460 Hz. The modulation index used in the PRI is used as the manipulated variable and the amplitude of the Ac output voltage across the parallel LC circuit is the controlled variable. The AC voltage output of the PRI is rectified by the doubler rectifier and the doubler rectifier, besides the reification action, also provides a voltage gain of 2. If the input voltage is 48 V and the gain

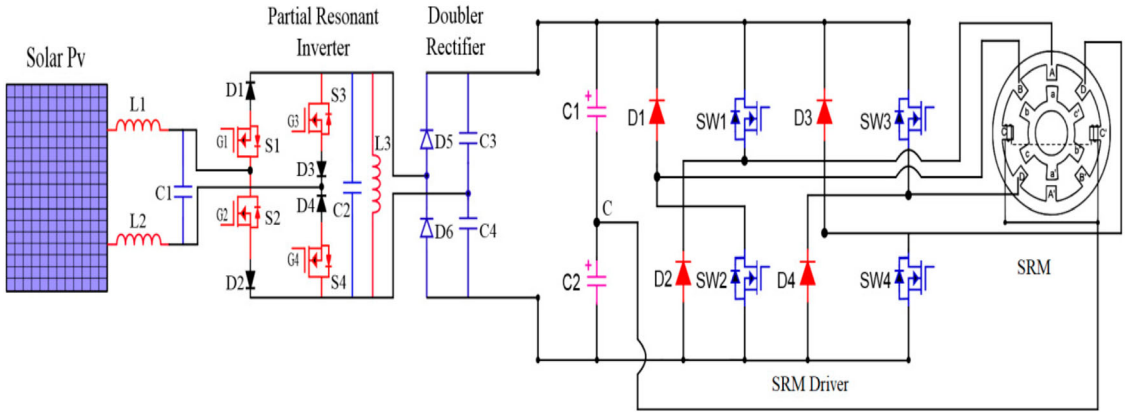

Figure 4. Flow chart of SMC-based MPPT.

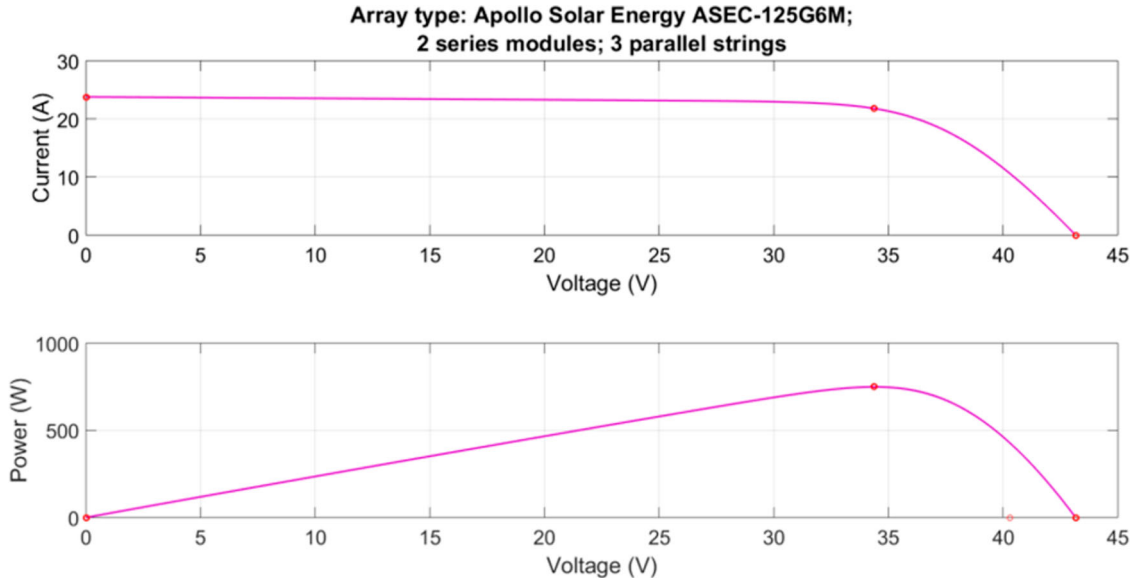

Figure 5. Topology of the proposed system.

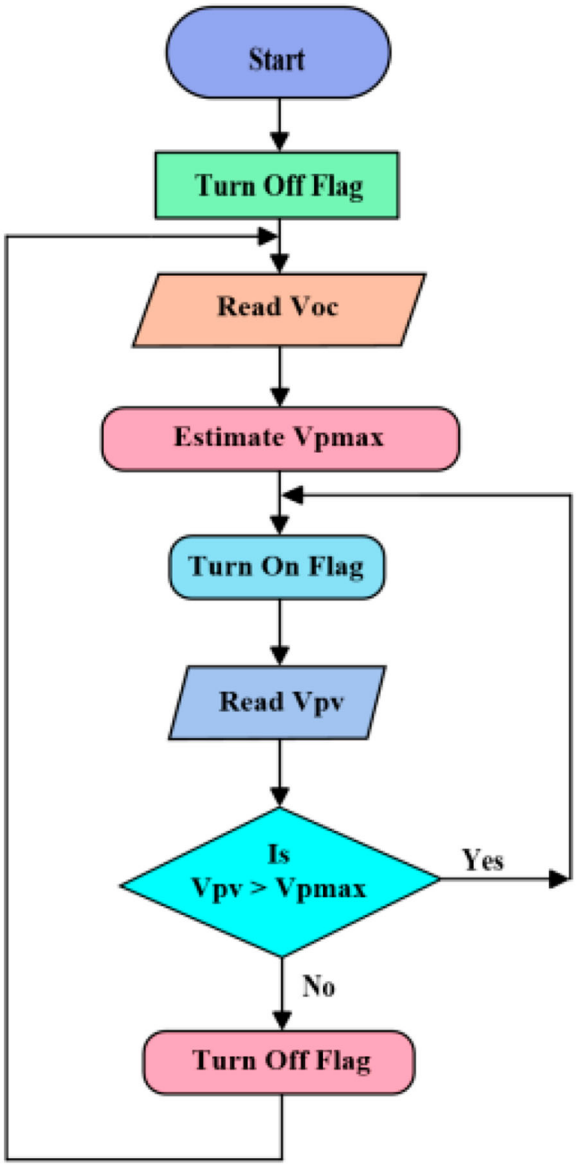

Figure 6. The energy E and co-energy E′.

of the PRI is 2.5 the doubler provides another voltage gain of 2 and the output voltage becomes DC 240 V.

4. MATLAB SIMULINK realization of proposed system

The proposed system was implemented in MATLAB SIMULINK and the various sub-systems and the results obtained are discussed in this section (Figure 6).

The specifications of the proposed system are shown in Table 2.

Figure 7 shows the main page of the MATLAB SIMULINK realization of the proposed system. The three sub-systems are the SPV sub-system, the PRI DR sub-system and the SRM and its drive subsystem. Figure 8 shows the arrangement of the SPV sub-system. The SMC-based MMPT is also included. The MPPT system generates a control flag that allows or stops the switching pulses for the switches of the PRI.

In the power converter system as shown in Figure 9, the PRI and the doubler rectifier are included. The doubler rectifier rectifies the resonant AC output of the PRI and delivers a voltage-doubled DC to the SRM driver. The DR consists of a set of two diodes and two capacitors. The topology of the PRI is shown in Figure 10. Four MOSFETS are arranged in the form of a bridge

Table 2. Specifications of components.

Parameter	Specification
Partial resonance inverter	
nominal input voltage	30–48 V
Output voltage	120 V AC
Switches	MOSFET 4 Nos
Power diodes	3 A 500 V 4 Nos
Doubler rectifier	
Power diodes	3 A 500 V 2 Nos
Capacitors	2500 MFD 2 Nos

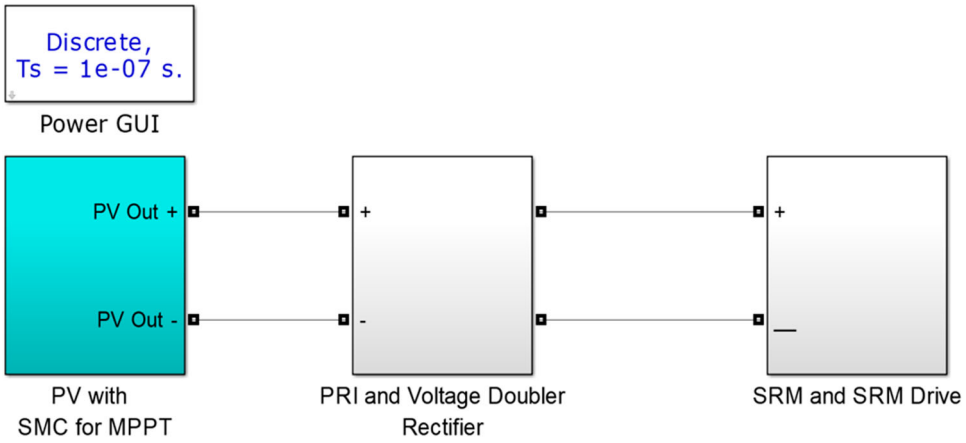

Figure 7. Overall implementation in MATLAB SIMULINK.

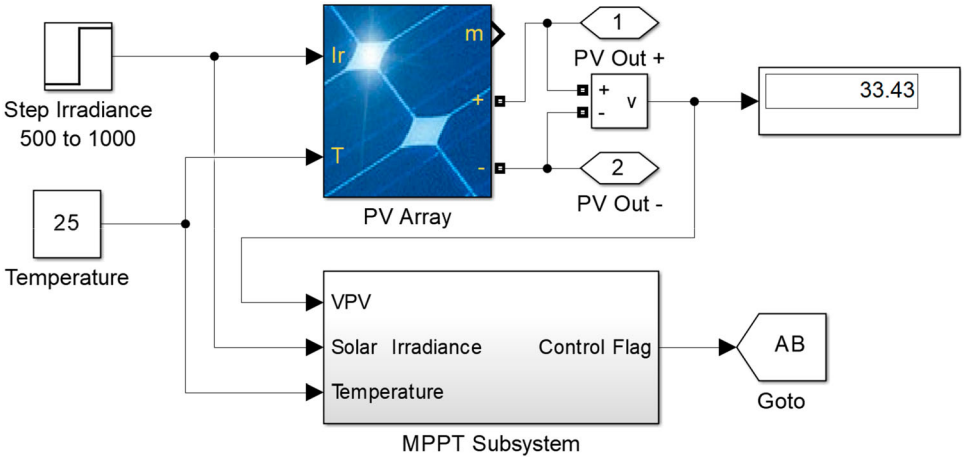

Figure 8. SPV module and the MPPT controller unit.

and reverse blocking diodes in series with each MOSFET. The DC supply is impressed across the nodes of the bridge and the DC rails deliver the AC output. Across the rails of the bridge is the parallel resonant LC parallel circuit is connected. Since the AC link voltage is more than the input DC voltage the reverse blocking diodes in series with each MOSFET are necessary.

Figure 11 shows the switching pulse generating subsystem for the switches of the PRI. A set of phase-shifted triangular carrier waves of frequency 8640 Hz are compared against a fixed modulation index of 0.45. The MPPT scheme gives a control flag that allows or stops the switching pulses to the MOSFETs of the PRI.

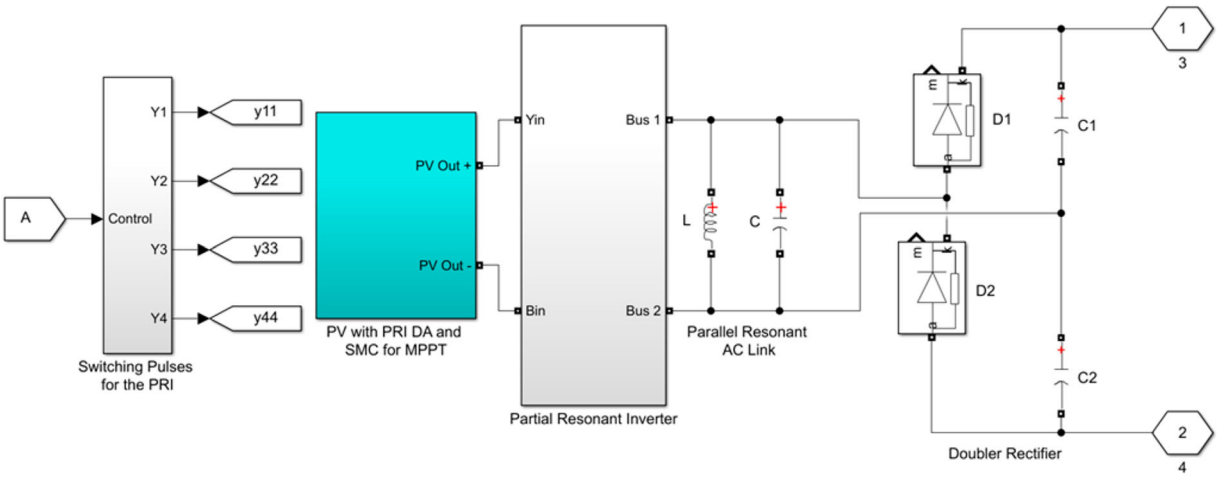

Figure 9. The PRI and the DR sub-system.

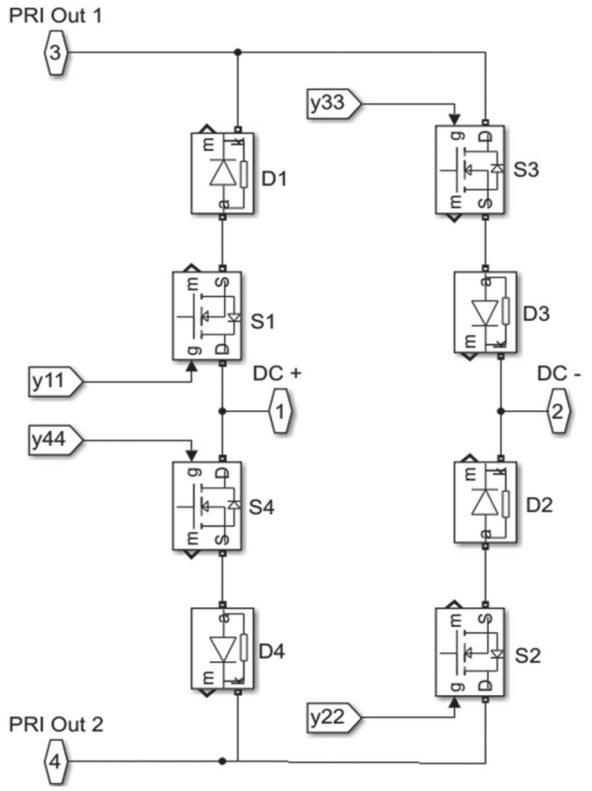

Figure 10. The topology of the PRI.

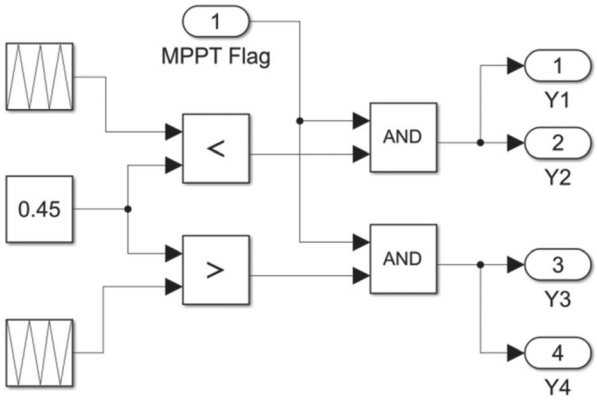

Figure 11. Switching pulse generation for the PRI.

The third subsystem is the SRM drive sub-system and the topology of the SRM drive subsystem is shown in Figure 12.

Figure 13 shows the SRM and the associated timing and measurement sub-systems. The switching pulses generated by the switches of the SRM follow the position sensor. The position signals from the motor are supplied to a timing system and the timing system produces the switching pulses. The internal structure of the timing unit is shown in Figure 14. Some parameter measurements and the scheme for converting the speed in radians per second to RPM are shown in Figure 15.

The display system is shown in Figure 15. The speed in radians per second is converted into RPM by a multiplication factor of 9.55.

A stability analysis of the proposed power conversion system was carried out. The input to the system is the voltage from the solar PV source and the output is the speed of the SRM. There is no bulk energy storage system like a battery used between the source and the load. The modulation index is kept fixed at 0.45. Therefore, the variables are the input voltage and the corresponding speed of the motor since the torque is also constant.

The transfer function of the system relating the speed of the SRM and the input voltage was considered useful to have an insight into the system and was derived using the command line commands of MATLAB. The system was run with a step change in the input voltage and the corresponding change in the speed of the machine was obtained. The input voltage and the speed of the machine were both sent to the workspace when the simulation was running. The variables "in" and "out" were respectively used for the input voltage and speed. The following commands were invoked and the transfer function was obtained.

> mysys = iddata (out, in, 0.0001)
> sys = tfest (mysys,2) and the transfer function obtained is given in Equation (6).

$$sys = (156.3s + 8213)/(S2 + 62.64s + 156.6) \ldots \quad (6)$$

By invoking the basic commands such as step, Rlocus and bode the control system studies were carried out and the plots obtained are presented in Figures 16–18, respectively. With regard to Figure 16, which is the step response of the transfer function between the source voltage and the speed, the system behaves like a first-order system and is stable in converging to the final steady state. The bode plot does not show up any peaks and it also shows sufficient phase and gain margins. This implies that the speed of the unmanned SRM will smoothly move up and down as the solar irradiance rises and falls. The error locus shown in Figure 18 confirms that there is no singularity and the poles and zeros of the system both lie on the negative half side of the complex plane. The system is, therefore, amenable to the development of nonlinear controllers like the sliding mode controller, or any linear controllers like the PI or Fuzzy logic controllers. However, since in this work, no energy storage system is involved an unregulated output voltage that is a function of the solar irradiance is applied to the SRM and the SRM-driven pump will deliver water with a pumping rate that directly depends upon the solar irradiance. No closed-loop controller except the MPPT for the SPV system is used in this work.

Some of the results of the simulation are presented herein. A step change in solar irradiance from

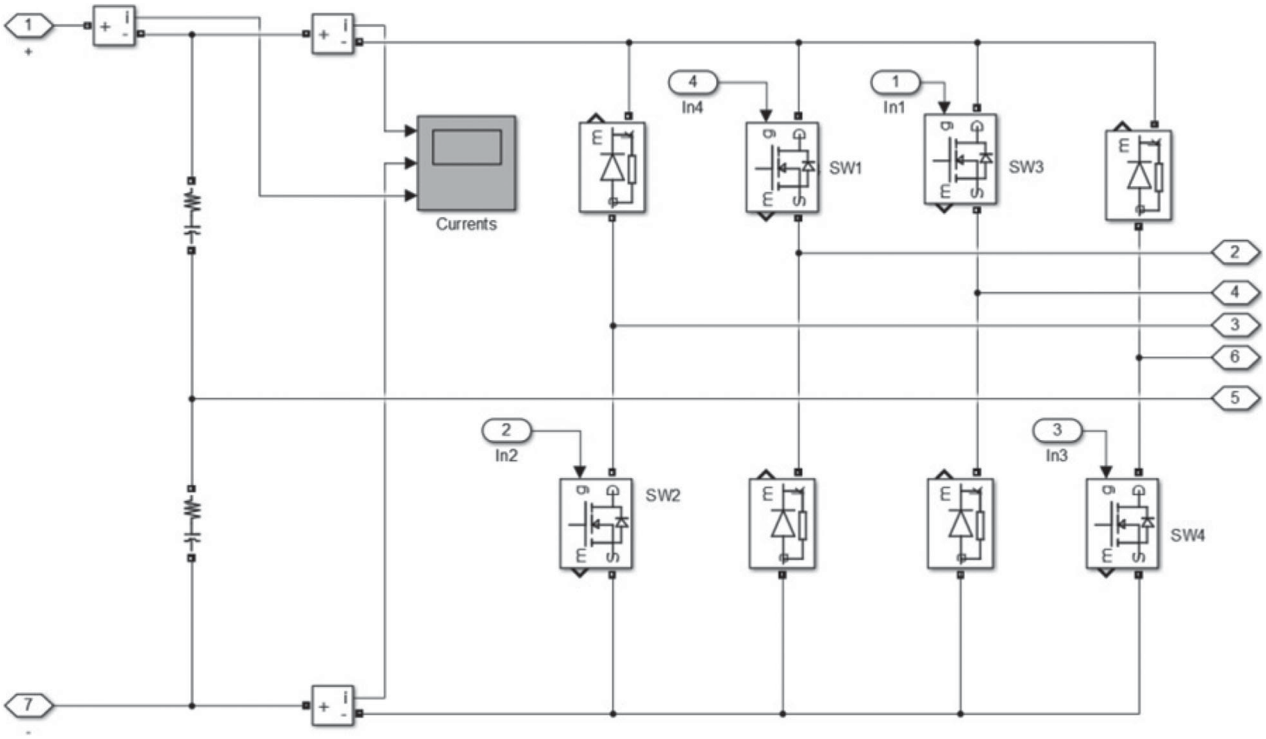

Figure 12. Topology of the SRM drive subsystem.

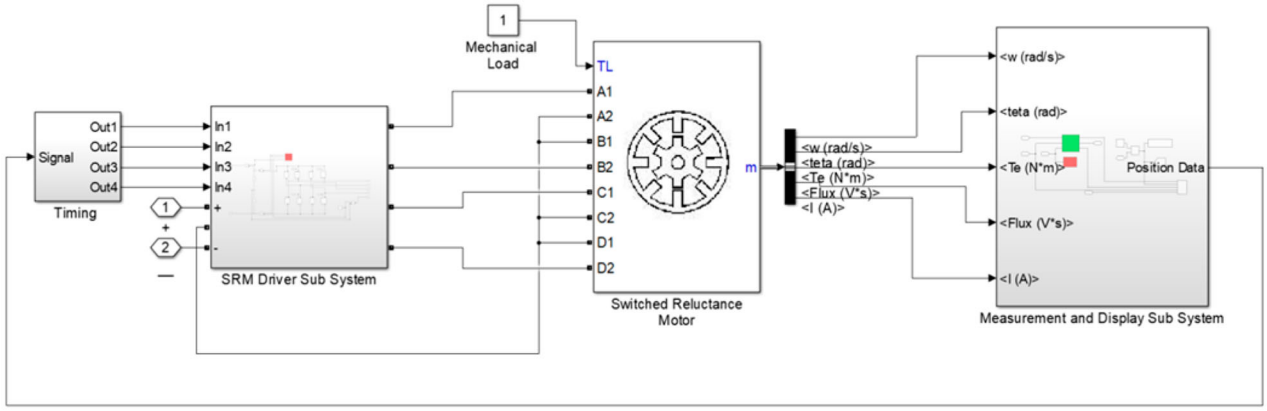

Figure 13. The SRM and timing and measurement subsystems.

500 W/m^2 to 1000 W/m^2 was introduced at 2 s. The change in the solar irradiance and the resulting change in the terminal voltage of the SPV are shown in Figure 19. With an active MPPT control, the variations in solar irradiance cause changes in the power harvested and it is routed into the PRI and then to the SRM through the SRM drive circuit. Since no energy storage system is used in this work and the load torque on the SRM is considered to be a constant, typically a water pump, the speed of the SRM changes following the changes in solar irradiance.

The power harvested by the solar PV system is supplied to the PRI and the switches of the PRI are supplied with switching pulses as shown in Figure 20. This causes a partial resonance and the partially resonant AC voltage across the AC link is shown in Figure 21. The output of the PRI is rectified and doubled by the doubler rectifier and the output of the doubler rectifier is shown in Figure 23. The current drawn by the PRI from the source side is shown in Figure 22.

The DC link voltage is obtained across the output of the doubler rectifier and is applied to the DC input terminals of the SRM drive circuit. It has been observed that the change in the solar irradiance from 500 W/m^2 to 1000 W/m^2 has caused the DC voltage to change from 180 V to 240 volts with a previous sudden rise of voltage from 0 V which is the initial state.

The resonant AC link has two main components, namely, the inductor L and the capacitor C. The current incoming to the AC link, the currents through the L and C and the current leaving the AC link and to the SRM drive are shown in Figure 24. The power transfer mechanism follows the principle that in each switching cycle over a short period, decided by the modulation index, initially energy is drawn from the source and is stored momentarily in the inductor and then it is transferred

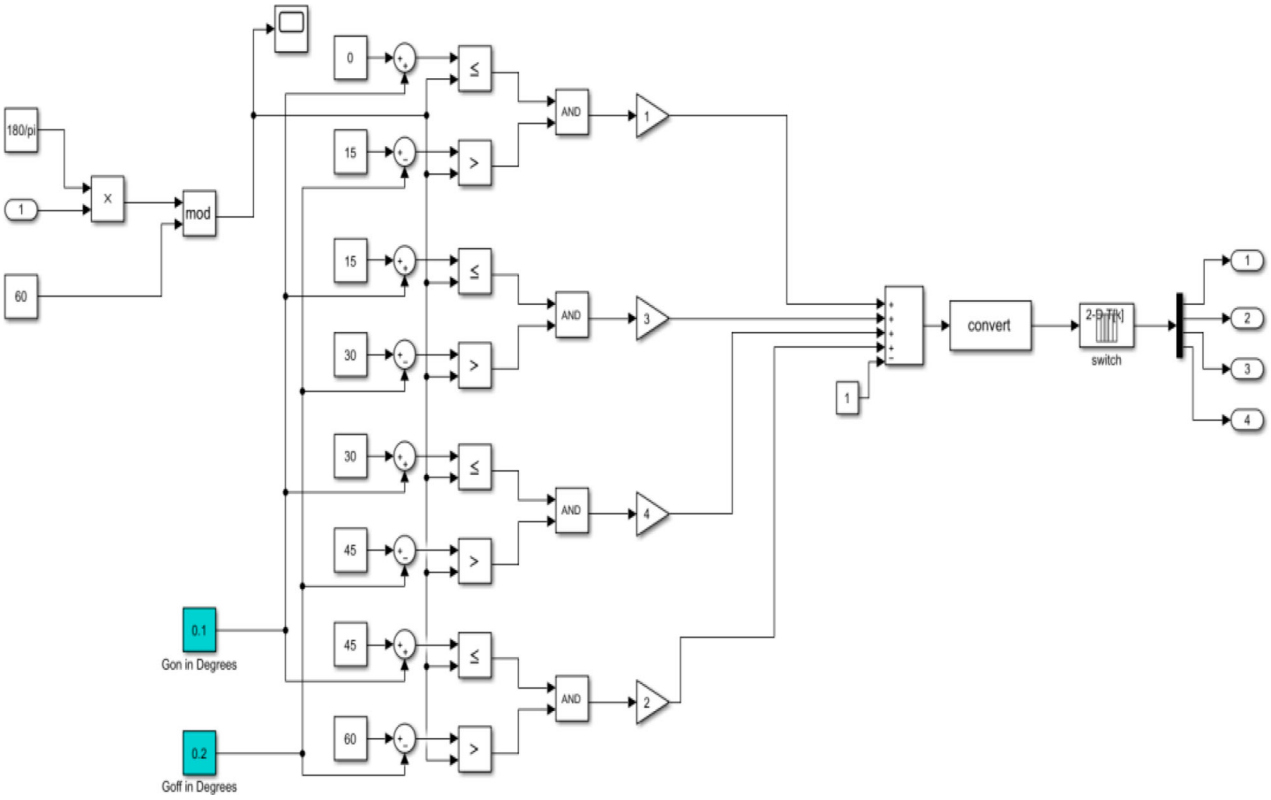

Figure 14. The timing unit used for generating the switching pulses for the four switches of the SRM drive.

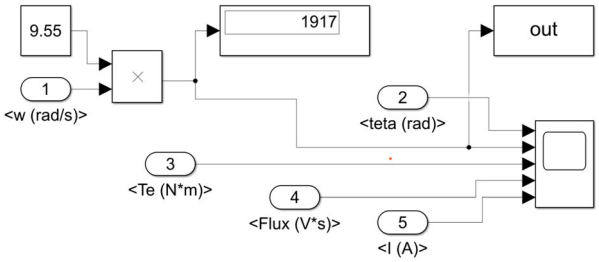

Figure 15. Monitoring of speed and other vital parameters.

to the load side. In an ideal parallel resonant circuit, the incoming current and the outgoing current should be equal as the inductor and capacitor currents cancel each other. However, because of the partial resonance phenomena and the local oscillations, the waveforms of the source side current and the load side current are different.

Figure 25 shows the trajectory of the speed of the SRM that is actually dictated by the changes occurring in the solar irradiance. In this experience, the initial solar irradiance is 500 W/m^2 and it jumps to 1000 W/m^2. Eventually, the speed of the SRM also undergoes a step change as shown in Figure 25. The other parameters of the SRM such as the angular position of the shaft, the torque, the flux linkage and phase currents are shown in Figure 26.

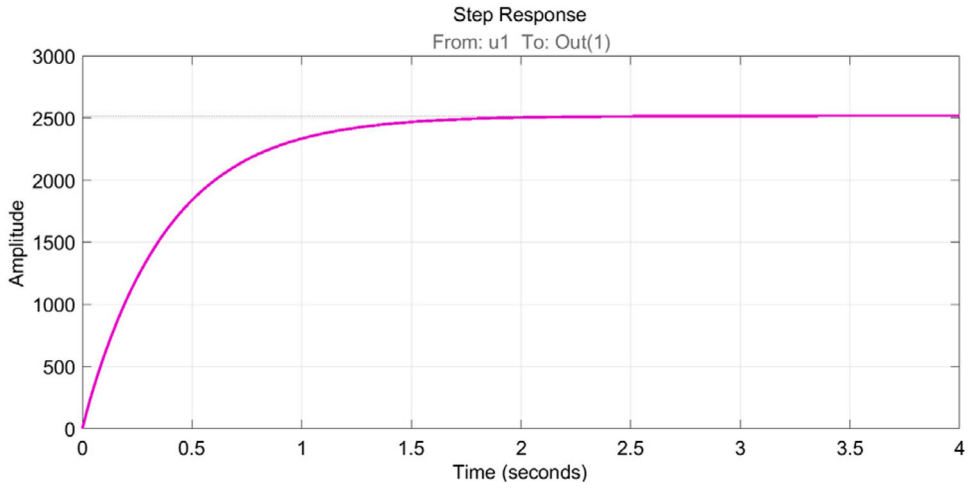

Figure 16. Step response of the transfer function.

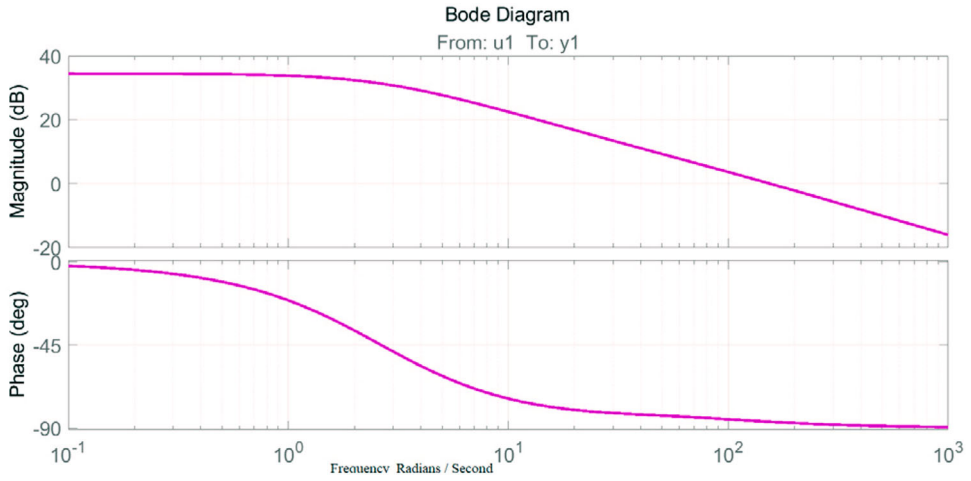

Figure 17. Bode plot of the transfer function.

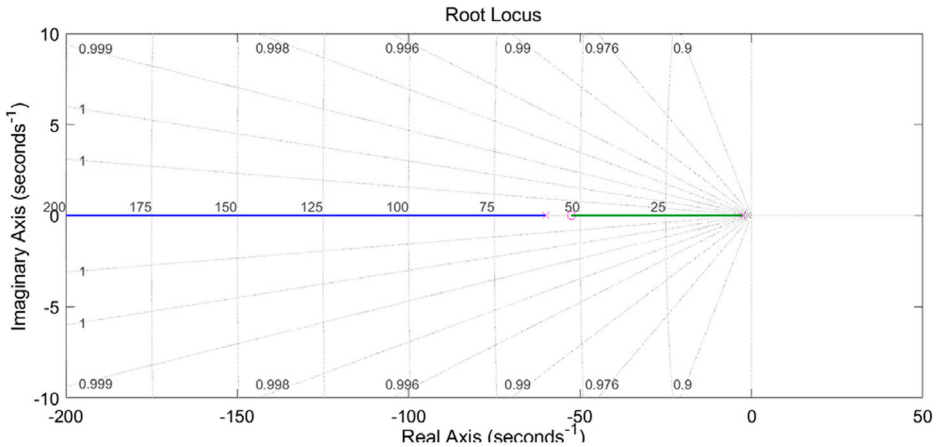

Figure 18. Root locus of the transfer function.

5. Experimental verification

An experimental verification prototype was built to validate the proposed idea of the PRI DR interface between the solar PV source and the SRM. Figure 27 shows the picture view of the experimental set-up. The proposed experimental set-up had been developed with the component values the same as that used for the simulations. MOSFETs were used for all the power electronic switches. The MOSFETs used in the PRI were of type IRF 540 and those used in the SRM drive were of type IRF840. All the MOSFETs received the pulses from the PIC micro-controller 1F877A. Separate PI 16F877A was used for the PRI and the SRM drive. The switching

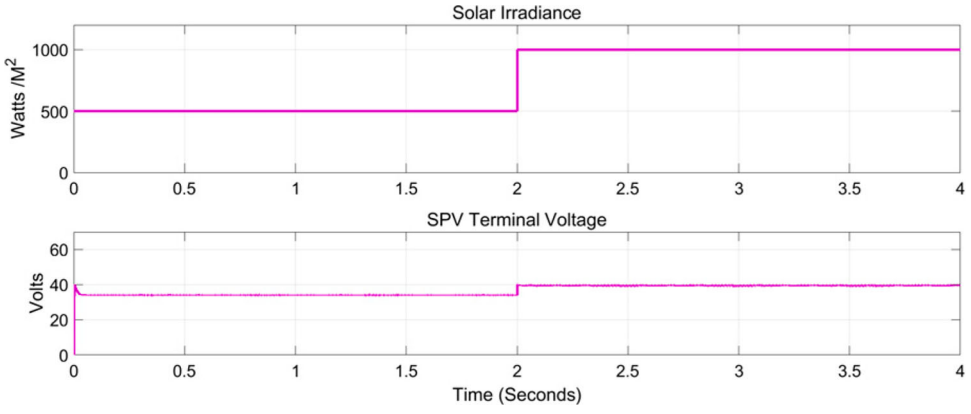

Figure 19. A step change in solar irradiance and the corresponding change in the SPV terminal voltage.

Figure 20. Switching pulses for the PRI switches.

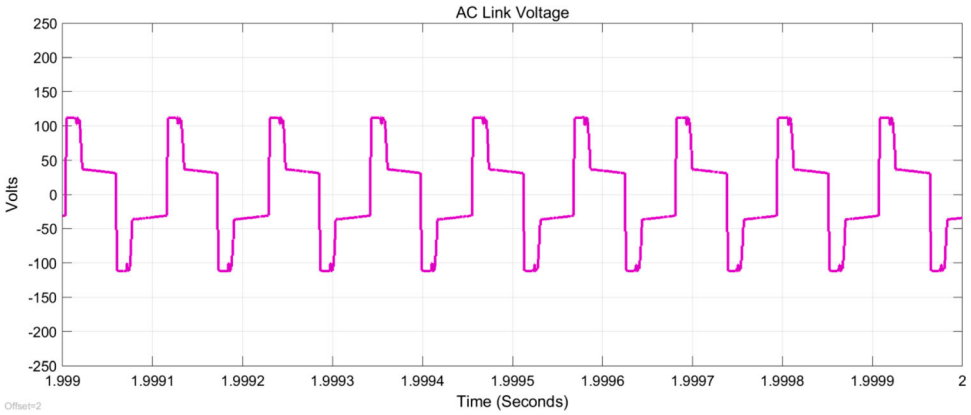

Figure 21. The AC link voltage.

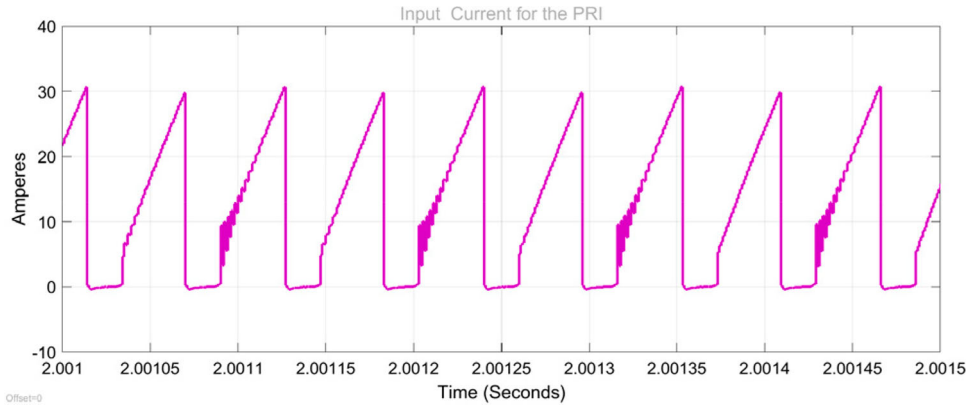

Figure 22. The input current or source current for the PRI.

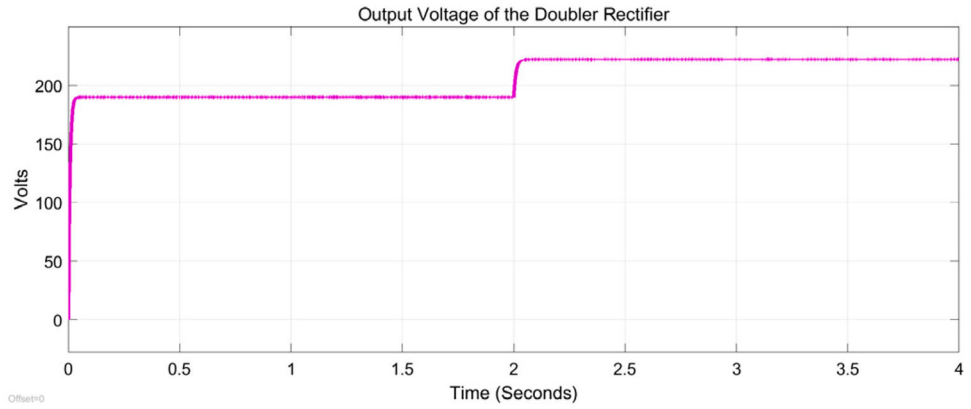

Figure 23. The DC link voltage.

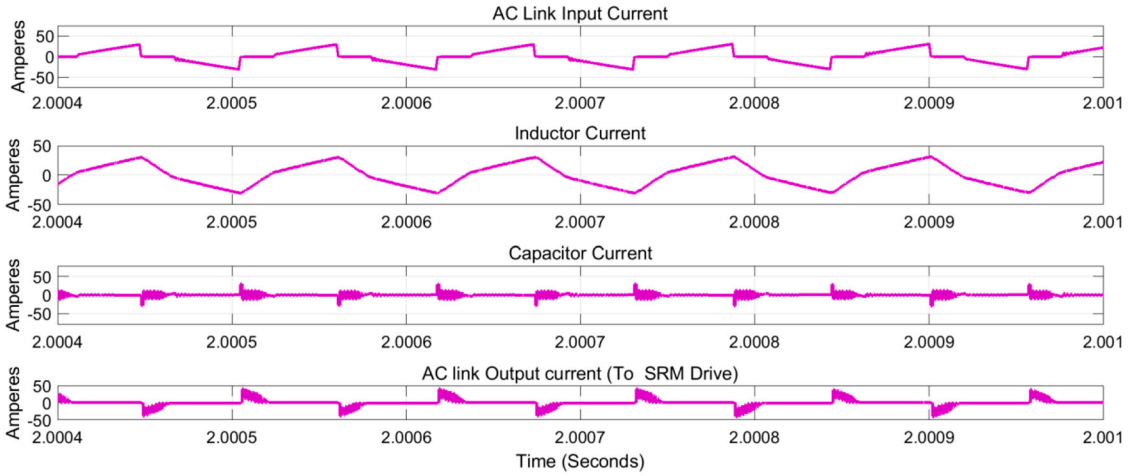

Figure 24. The currents associated with the AC link.

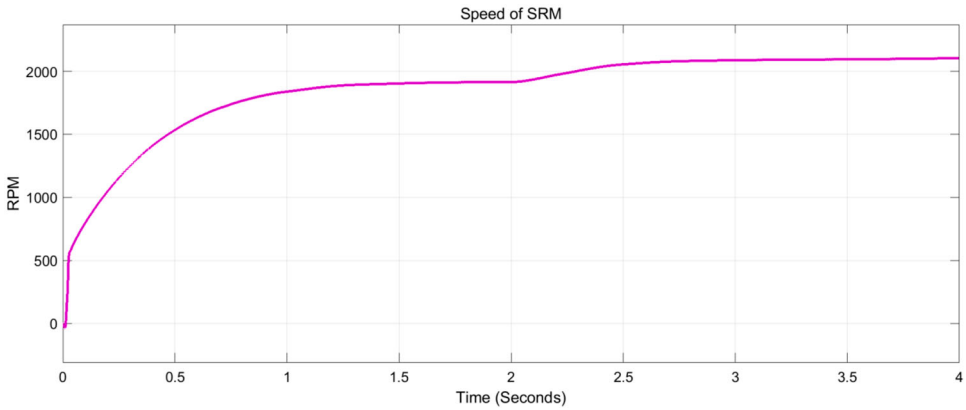

Figure 25. The trajectory of the speed of the SRM as the Solar Irradiance suddenly changes at 2 s.

pulses from the PIC micro-controller were applied to the MOSFETs through opto coupler-type MCT2E.

Some of the important waveforms observed from the experimental prototype are presented herein. Figure 28 shows the switching pulse used in the PRI section. The partial resonant AC link voltage produced by the PRI is shown in Figure 30. The doubler rectifier rectifies the resonant AC link and produces a steady DC voltage.

The SRM drive timing circuit realized using the PIC16F877A accepts the position sensor output and generates the switching pulses for the switches of the drive for the SRM. The position sensor output is shown in Figure 31. The switching pulses for the SRM switches are shown in Figure 32.

The variation in solar irradiance was observed as a variation in the terminal voltage of the SPV panel as

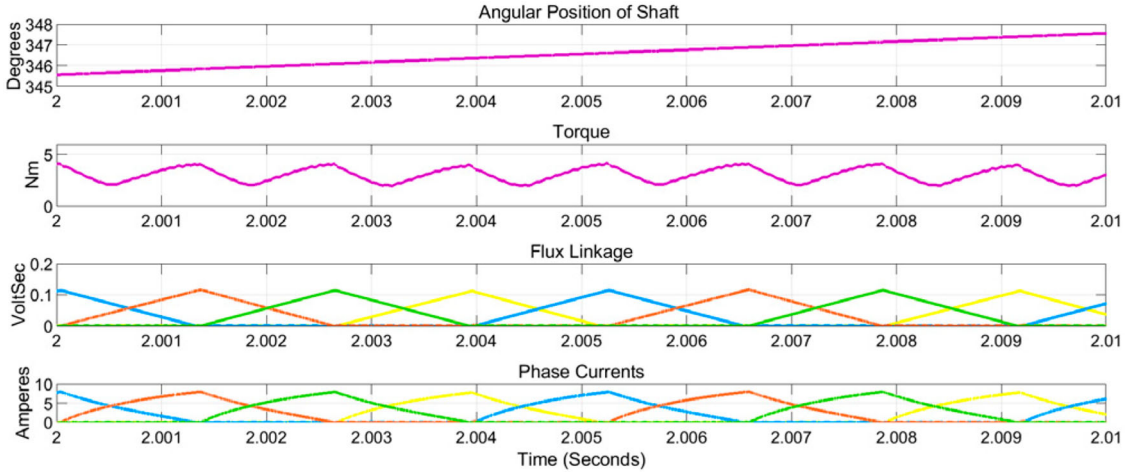

Figure 26. Waveforms associated with the SRM.

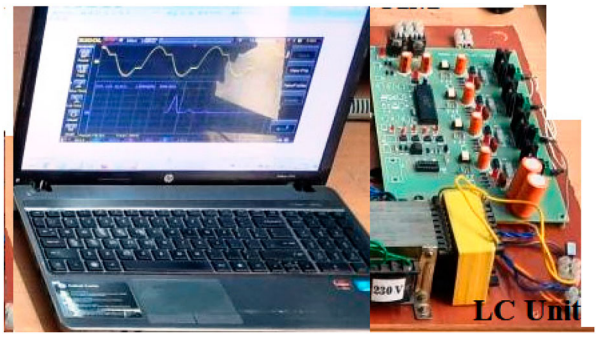

Figure 27. Some photographs of the PRI.

shown in Figure 33. The resulting speed of the SRM as measured by using a tacho generator is shown in Figure 34. The results confirm that the proposed idea offers better voltage boost behaviour, it is stable and reliable power conversion efficiency of 82.5% which is comparable to that of the super lift Luo converter used for the same purpose where the power conversion efficiency was 88%. Thus the proposed idea can be a better choice for the voltage step operation where the source voltage is too low while the motor requires a high voltage as high as 5–10 times the source voltage.

6. Conclusion

In this work, a novel Dc-to-Dc converter with a high voltage gain realized by a partial resonant inverter and a doubler rectifier has been proposed and validated. The proposed converter has been powered by a solar PV source of 40 V nominal power rating

Figure 28. Switching pulses for the opposite switches of PRI.

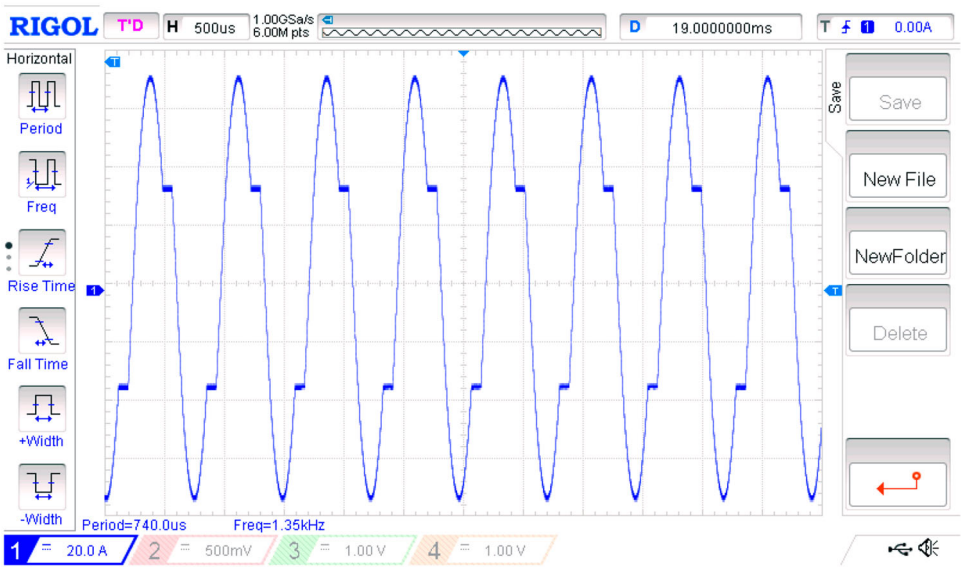

Figure 29. The partial resonant AC link voltage.

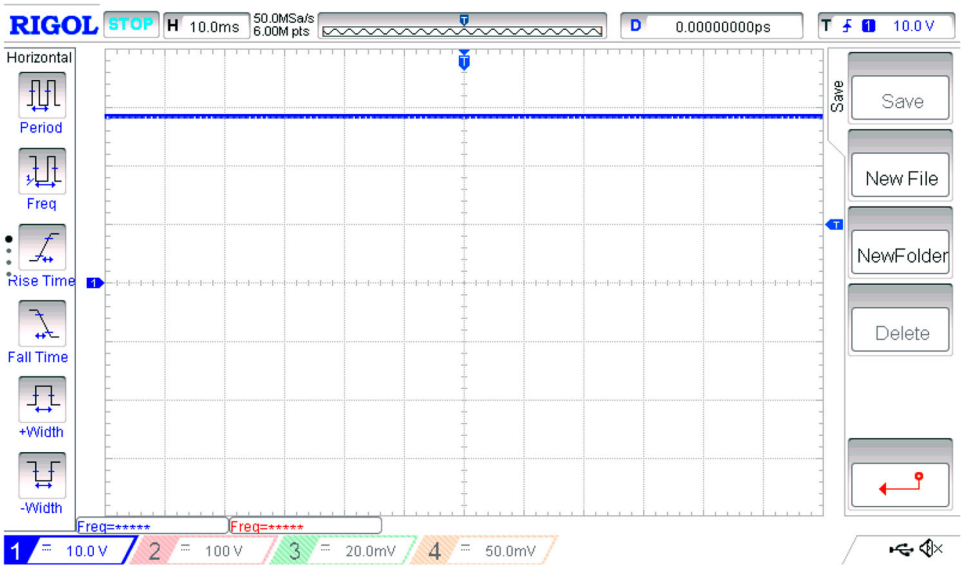

Figure 30. The DC link voltage of 150 V (5:1).

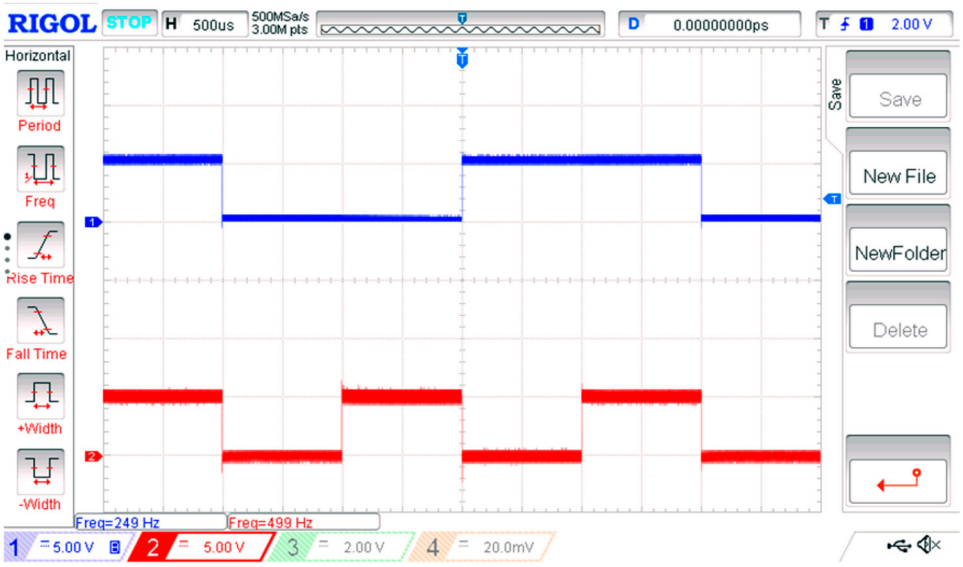

Figure 31. Two-bit position sensor output.

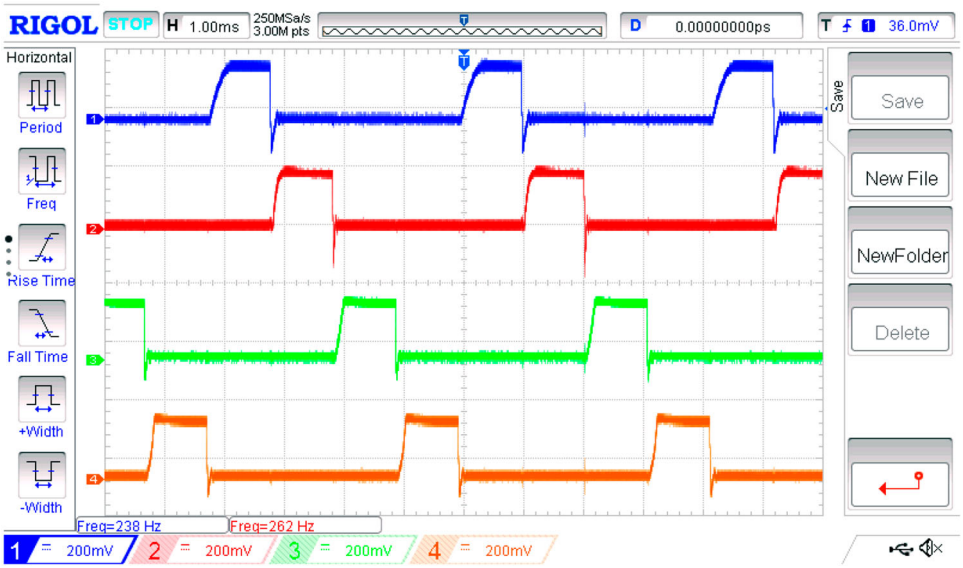

Figure 32. Switching pulses for the SRM.

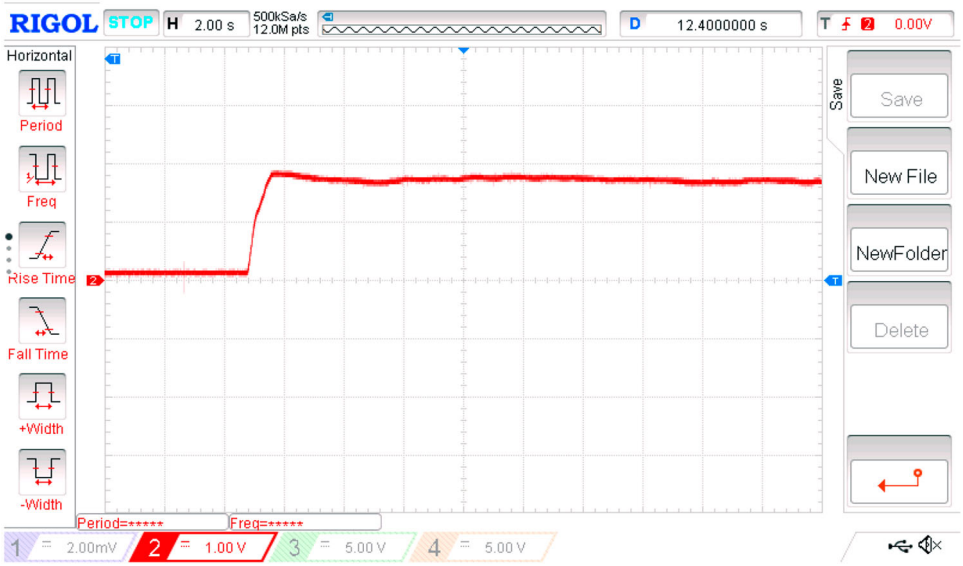

Figure 33. Terminal voltage of SPV (20:1).

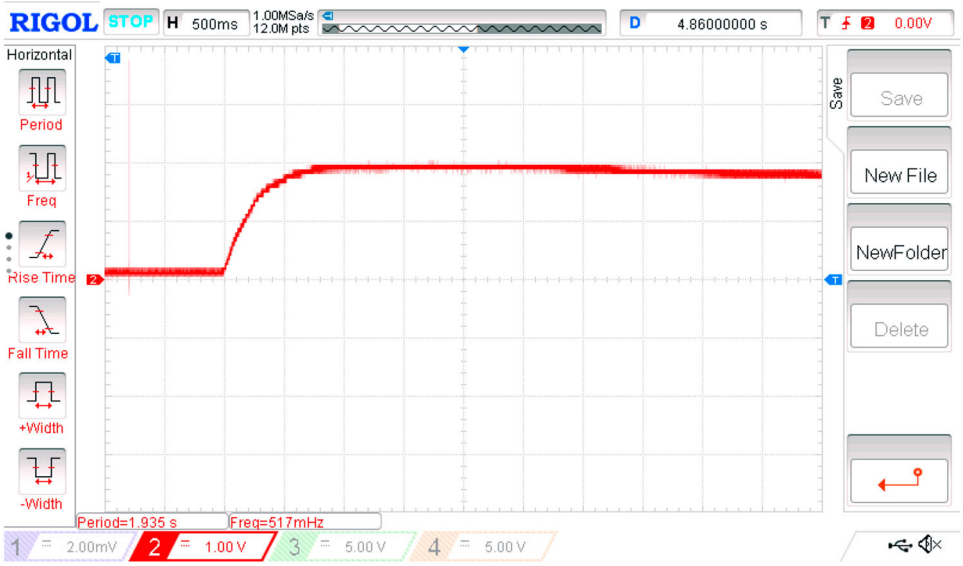

Figure 34. Speed of SRM.

and it was stepped up to as high as 240 V to drive a switched reluctance motor that drives a remote water pumping system. It has been observed that the speed of the SRM is a function of solar irradiance. The proposed system has been validated by a suitable circuit model in MATLAB and an experimental prototype as well, the results of the simulations and the experimental prototype have validated the proposed idea. In future works, it might be possible to study another renewable energy system, such as wind energy or fuel cells that uses the proposed converter and the new controlled strategy with the whole system.

Disclosure statement

No potential conflict of interest was reported by the author(s).

References

[1] Gopal C, Mohanraj M, Chandramohan P, et al. Renewable energy source water pumping systems—a literature review. Renew Sustain Energy Rev. 2013;25:351–370. doi:10.1016/j.rser.2013.04.012

[2] Park SS, Cho GH. October. A current regulated pulse width modulation method with new series resonant inverter. In: Conference record of the IEEE industry applications society annual meeting. IEEE; 1989. p. 1045–1051.

[3] Moo CS, Chuang YC, Lee CR. A new power-factor-correction circuit for electronic ballasts with series-load resonant inverter. IEEE Trans Power Electron. 1998;13(2):273–278. doi:10.1109/63.662839

[4] Pantic Z, Bai S, Lukic SM. ZCS $ LCC $-compensated resonant inverter for inductive-power-transfer application. IEEE Trans Ind Electron. 2010;58(8):3500–3510. doi:10.1109/TIE.2010.2081954

[5] Krishnan R. Switched reluctance motor drives modelling. London: CRC Press; 2001.

[6] Fitzgerald AE, Kingsley C, Umans SD. Introduction to rotating machines. In: Electric machinery. McGraw-Hill; 2014. p. 216–222.
[7] Baishya, R. Unique solution of unpolarized evolution equations. Int J Res Appl Sci Eng Technol. 2020;8(4):499–509.
[8] Ananda Padmanaban L, Saravanan P. Design, analysis and comparison of switched reluctance motors for electric vehicle application. Automatika. 2022;64(2):239–247. doi:10.1080/00051144.2022.2140388
[9] Lee JY, Lee BK, Sun T, et al. Dynamic analysis of toroidal winding switched reluctance motor driven by 6-switch converter. IEEE Trans Magn. 2006;42(4):1275–1278. doi:10.1109/TMAG.2006.871933
[10] Kocan S, Rafajdus P. Dynamic model of high speed switched reluctance motor for automotive applications. Transp Res Proc. 2019;40:302–309. doi:10.1016/j.trpro.2019.07.045
[11] Ishikawa T, Hashimoto Y, Kurita N. Optimum design of a switched reluctance motor fed by asymmetric bridge converter using experimental design method. IEEE Trans Magn. 2014;50(2):781–784. doi:10.1109/TMAG.2013.2285584
[12] Bukhari AAS, Alalibo BP, Cao W, et al. Switched reluctance motor design for electric vehicles based on harmonics and back EMF analysis. J Eng. 2019;2019(17):4220–4225. doi:10.1049/joe.2018.8194
[13] Vijayakumar K, Karthikeyan R, Paramasivam S, et al. Switched reluctance motor modeling, design, simulation, and analysis: a comprehensive review. IEEE Trans Magn. 2008;44(12):4605–4617. doi:10.1109/TMAG.2008.2003334
[14] Lan Y, Benomar Y, Deepak K, et al. Switched reluctance motors and drive systems for electric vehicle powertrains: state of the art analysis and future trends. Energies. 2021;14(8):2079. doi:10.3390/en14082079
[15] Ahn JW, Lukman GF. Switched reluctance motor: research trends and overview. CES Trans Electric Mach Syst. 2018;2(4):339–347. doi:10.30941/CESTEMS.2018.00043
[16] Krishnan R, Park SY, Ha K. Theory and operation of a four-quadrant switched reluctance motor drive with a single controllable switch-the lowest cost four-quadrant brushless motor drive. IEEE Trans Ind Appl. 2005;41(4):1047–1055. doi:10.1109/TIA.2005.851019
[17] Pathak PK, Yadav AK. Design of battery charging circuit through intelligent MPPT using SPV system. Sol Energy. 2019;178:79–89. doi:10.1016/j.solener.2018.12.018
[18] Gulig PA, Danbara H, Guiney DG, et al. Molecular analysis of spv virulence genes of the salmonella virulence plasmids. Mol Microbiol. 1993;7(6):825–830. doi:10.1111/j.1365-2958.1993.tb01172.x
[19] Purohit P, Michaelowa A. CDM potential of SPV pumps in India. Renew Sustain Energy Rev. 2008;12(1):181–199. doi:10.1016/j.rser.2006.05.011
[20] Bana S, Saini RP. A mathematical modeling framework to evaluate the performance of single diode and double diode based SPV systems. Energy Rep. 2016;2:171–187. doi:10.1016/j.egyr.2016.06.004
[21] Manoj Kumar P, Mukesh G, Naresh S, et al. Study on performance enhancement of SPV panel incorporating a nanocomposite PCM as thermal regulator. In: Mohan S., Shankar S., Rajeshkumar G, editors. Materials, design, and manufacturing for sustainable environment. Lecture Notes in Mechanical Engineering. Singapore: Springer; 2021. p. 587–597. doi:10.1007/978-981-15-9809-8_44
[22] Valappil SP, Misra SK, Boccaccini AR, et al. Large-scale production and efficient recovery of PHB with desirable material properties, from the newly characterised bacillus cereus SPV. J Biotechnol. 2007;132(3):251–258. doi:10.1016/j.jbiotec.2007.03.013
[23] Khan FA, Pal N, Saeed SH. Optimization and sizing of SPV/wind hybrid renewable energy system: A techno-economic and social perspective. Energy. 2021;233:121114. doi:10.1016/j.energy.2021.121114
[24] Thakran S, Singh J, Garg R, et al. Implementation of P&O algorithm for MPPT in SPV system. 2018 *international conference on power energy, environment and intelligent control (PEEIC)*. Greater Noida: IEEE; 2018 Apr. p. 242–245. doi:10.1109/PEEIC.2018.8665588
[25] Agarwal RK, Hussain I, Singh B. Implementation of LLMF control algorithm for three-phase grid-tied SPV-DSTATCOM system. IEEE Trans Ind Electron. 2016;64(9):7414–7424. doi:10.1109/TIE.2016.2630659
[26] Jain C, Singh B. A three-phase grid tied SPV system with adaptive DC link voltage for CPI voltage variations. IEEE Trans Sustain Energy. 2015;7(1):337–344. doi:10.1109/TSTE.2015.2496297
[27] Naghavi F, Toliyat H. Grid-connected soft switching partial resonance inverter for distributed generation. *2022 IEEE 31st international symposium on industrial electronics (ISIE)*. Anchorage, AK: IEEE; 2022, June. p. 927–932. doi:10.1109/ISIE51582.2022.9831465
[28] Uno M, Kukita A. Two-switch voltage equalizer using an LLC resonant inverter and voltage multiplier for partially shaded series-connected photovoltaic modules. IEEE Trans Ind Appl. 2014;51(2):1587–1601. doi:10.1109/TIA.2014.2336980
[29] Sakthivel K, Krishnasamy R, Balasubramanian K, et al. A revolutionary partial resonant inverter and doubler rectifier with MPPT based on sliding mode controller for harvesting solar photovoltaic sources. Sustain Comp Inform Syst. 2022;36:100811. doi:10.1016/j.suscom.2022.100811
[30] Amirabadi M, Baek J, Toliyat HA. Bi-directional sparse parallel partial resonant ac-link inverter. 2013 Twenty-Eighth annual IEEE applied power electronics conference and exposition (APEC). Long Beach, CA: IEEE; 2013, March. p. 136–143. doi:10.1109/APEC.2013.6520198
[31] Vidhya C, Muralidharan S, Ravikumar V. Design of a partial resonant inverter for solar photovoltaic applications. Automatika. 2021;62(3-4):434–448. doi:10.1080/00051144.2021.1983697
[32] Amirabadi M, Toliyat HA. A new class of PV inverters: series partial resonant converters. In: 2012 IEEE energy conversion congress and exposition (ECCE). Raleigh, NC: IEEE; 2012, September. p. 3125–3132. doi:10.1109/ECCE.2012.6342509.